On the Behavior of Solutions of Xenon in Liquid *n*-Alkanes: Solubility of Xenon in *n*-Pentane and *n*-Hexane

Rui P. M. F. Bonifácio,[†] Luís F. G. Martins,[‡] Clare McCabe,[§] and Eduardo J. M. Filipe*,[†]

Centro de Química Estrutural, Instituto Superior Técnico, 1049-001 Lisboa, Portugal, Centro de Química de Évora, Universidade de Évora, Rua Romão Ramalho 59, 7000-671 Évora, Portugal, and Department of Chemical and Biomolecular Engineering, and Department of Chemistry, Vanderbilt University, Nashville, Tennessee 37235-1604, United States

The solubility of xenon in liquid *n*-pentane and *n*-hexane has been studied experimentally, theoretically, and by computer simulation. Measurements of the solubility are reported for xenon + *n*-pentane as a function of temperature from 254 to 305 K. The uncertainty in the experimental data is less than 0.15%. The thermodynamic functions of solvation such as the standard Gibbs energy, enthalpy, and entropy of solvation have been calculated from Henry's law coefficients for xenon + *n*-pentane solutions and also for xenon + *n*-hexane, which were reported in previous work. The results provide a further example of the similarity between the xenon + *n*-alkane interaction and the *n*-alkane + *n*-alkane interactions. Using the SAFT-VR approach we were able to quantitatively predict the experimental solubility for xenon in *n*-pentane and semiquantitatively that of xenon in *n*-hexane using simple Lorentz−Berthelot combining rules to describe the unlikely interaction. Henry's constants at infinite dilution for xenon + *n*-pentane and xenon + *n*-hexane were also calculated by Monte Carlo simulation using a united atom force field to describe the *n*-alkane and the Widom test particle insertion method.

1. Introduction

Mixtures involving *n*-alkanes and noble gases have been extensively studied and used as model systems for testing statistical theories of liquids. These chemical families provide a range of molecules whose physical properties gradually change within the homologous series or periodic group and are therefore especially suited to study the role of size, shape, and flexibility on the thermodynamic properties of liquid mixtures. The interaction between xenon and the *n*-alkanes, in particular, has been extensively studied. Xenon is highly soluble in lipids and fats and shows anesthetic properties at subatmospheric pressures. Given its chemical inertia, nontoxicity, and nonflammability (which make it an easy and safe gas to handle), xenon could be considered the perfect anesthetic; its use was recently submitted for regulatory medical approval in Europe.[1] A further important application of xenon in nuclear medicine involves the use of ^{133}Xe isotope to study cerebral blood flow and pulmonary functions.[2]

At the molecular level, xenon is a spherical and structureless particle, with a high polarizability that enhances dispersion forces. Its intermolecular potential is therefore relatively well characterized. These properties justify its frequent use as a prototype solute in the study of solute−solvent interactions from first principles. In addition, one of xenon's most abundant natural isotopes, [129]Xe, has an NMR-active nucleus whose shielding constant is very sensitive to the local environment. The [129]Xe particle can thus be used as a "probe" to study the properties of condensed phases, biological structures, and microporous materials by NMR spectroscopy.[3,4]

In previous work[5−7] we reported low-temperature thermodynamic studies (from 160 to 200 K) of mixtures of xenon with the lighter alkanes (methane, ethane, propane, butane, and *i*-butane). We found that these mixtures exhibit a behavior that closely resembles that seen for mixtures of *n*-alkanes. The data, as interpreted by the statistical associating fluid theory (SAFT-VR),[8] indicates that xenon can be represented by a sphere with almost the same diameter and intermolecular potential, as those suited to describe the *n*-alkanes. The diameter of the xenon atom (measured, for instance, in terms of its van der Waals radius) agrees very well with that of the cross-sectional diameter of the *n*-alkanes. The following example provides further evidence of this behavior, as do the results presented in this work.

Excess enthalpies (H^E) for a number of equimolar mixtures of *n*-alkanes are plotted in Figure 1a as a function of temperature. From the figure we observe the general trend that *n*-alkanes mix with positive excess enthalpies at low temperature, which decrease with increasing temperature, passing through zero, and becoming negative at higher temperatures. The temperature at which H^E ($x = 0.5$) becomes negative changes from system to system. Interestingly, if the same data is plotted against the reduced temperature of the mixtures, $T_{c_{12}}$ (defined as $T_{c_{12}} = (1 - k_{12})(T_{c_1}T_{c_2})^{1/2}$, where $(1 - k_{12}) = (8(V_{c_1}V_{c_2})^{1/2})/((V_{c_1}^{1/3} + V_{c_2}^{1/3})^3)$ and T_{c_1}, T_{c_2}, V_{c_1}, and V_{c_2} are, respectively, the critical temperatures and critical volumes of the pure fluids) it can be observed that the temperature at which H^E ($x = 0.5$) becomes negative falls within 0.57 and 0.59 for all systems (Figure 1b). Following our suggestions,[9,10] Blas and dos Ramos[11] were able to reproduce this universal behavior using the *soft*-SAFT equation. The reduced temperature at which H^E ($x = 0.5$) becomes negative was predicted by theory as 0.51−0.52.
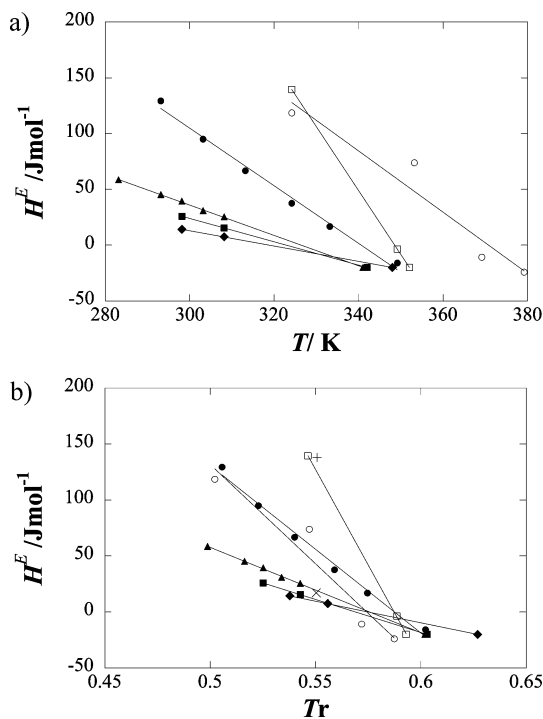
Also included in Figure 1b are the H^E ($x = 0.5$) values for the xenon + propane and xenon + *n*-butane systems. Given

* To whom correspondence should be addressed. E-mail: efilipe@ist.utl.pt.
† Instituto Superior Técnico.
‡ Universidade de Évora.
§ Vanderbilt University.

a)

b)

Figure 1. Excess enthalpies, H^E ($x = 0.5$), for equimolar mixtures of *n*-alkanes and xenon + *n*-alkanes as a function of (a) temperature and (b) reduced temperature. Lines are trend lines, and symbols are experimental data from the literature: (◆) *n*-hexane + *n*-decane, (■) *n*-hexane + *n*-undecane, (▲) *n*-hexane + *n*-dodecane, (●) *n*-hexane + *n*-hexadecane, (□) *n*-hexane + *n*-tetracosane, (○) *n*-octane + *n*-octacosane, (+) xenon + propane, (×) xenon + *n*-butane.

the volatility of these compounds, the experimental data for these mixtures was determined at much lower temperatures. Nevertheless, the xenon + alkane data conforms to the general *n*-alkane + *n*-alkane trend.

As it will be shown, the results reported in this work provide further evidence supporting that these findings are not mere coincidences at the macroscopic level but reflect a more universal behavior at the molecular level.

Solubility measurements often constitute an important source of information about the properties and structure of solutions.[12] Precise measurements covering sufficiently large ranges of temperature are frequently the only means of obtaining the enthalpy and heat capacity changes associated with the dissolution process. In the present work, accurate determinations of the solubility of xenon in *n*-pentane as a function of temperature have been performed in the 254−304 K range. From the experimental results, thermodynamic quantities of solvation were calculated for both xenon + *n*-pentane and xenon + *n*-hexane, which was measured in previous work.[13] As before,[14] the systems were modeled using the SAFT-VR approach. Henry's constants at infinite dilution as a function of temperature were also obtained by molecular simulation and are directly compared with experimental results.

2. Experimental Section

The *n*-pentane solvent was obtained from Lab-Scan, analytical reagent, with a 99% mol/mol minimum stated purity. The liquid was purified by distillation in an inert atmosphere of dry nitrogen. The final purity was confirmed by checking its vapor pressure after degasification. Deviations from literature values[15] were found to be less than 0.1%. The xenon used was from

TABLE 1: Values for the Henry's Law Coefficients, Equilibrium Pressure, p, and Xenon Molar Fraction in Gaseous and Liquid Phases between 254 and 305 K for Xenon + *n*-Pentane solutions

T/K	p/kPa	x_2 (10^{-2})	y_2	$H_{2,1}$ (p_1^{sat}, T)/MPa
254.19	66.90	3.0384	0.8620	1.886
255.77	68.80	2.9841	0.8538	1.956
258.35	71.83	2.9118	0.8395	2.058
267.30	83.75	2.6726	0.7842	2.443
269.36	86.96	2.6115	0.7706	2.551
277.69	101.2	2.4040	0.7114	2.978
279.96	105.5	2.3515	0.6944	3.101
286.22	118.9	2.2053	0.6470	3.475
295.17	141.8	2.0219	0.5777	4.040
304.48	171.4	1.8413	0.5074	4.718

Linde Gas with 99.99% mol/mol minimum stated purity. The gas was used as received from the manufacturer.

The experimental apparatus and procedure have been previously described in detail.[12] The solubility measurements involve equilibration of known amounts of dry gas and degassed solvent at constant volume and determination of the equilibrium pressure for the saturated solution maintained at constant temperature.

The amount of gas is determined by measuring its pressure in a calibrated glass bulb at constant temperature and correcting for gas imperfection. Pressure is measured with a transducer (Paroscientific model 0-7 bar, precision 0.01% FS). The pure solvent is degassed by successive melting/freezing cycles while vacuum pumping noncondensable gases. The amount of pure solvent is determined volumetrically. The equilibrium cell, based on the design of Carnicer,[16] has two capillaries through which the liquid is forced to circulate during the equilibration process, promoting a close contact with the gas. The volume of the cell was previously determined with a precision of 0.01%. The readings of pressure during the dissolution process are recorded until a constant value is reached, indicating that equilibrium has been attained. The final pressure, temperature, and level of the solution in the capillaries are then measured. Equilibrium is typically attained within 72 h.

Temperature is maintained constant in a water thermostat to within 0.01 K by means of a Hart Scientific PID temperature controller and is measured with a previously calibrated Pt100 platinum resistance thermometer. The measurement of solubility at different temperatures is done by simply changing the thermostat set point and waiting for a new thermodynamic equilibrium. With a single loading it is thus possible to make measurements over a large temperature range. Several runs, in which the temperature was both increased and decreased, were performed in order to check the reproducibility of the results.

3. Experimental Results

The solubility of xenon in *n*-pentane was experimentally measured from 254.19 to 304.48 K. The results are reported in Table 1. For each experimental point, the temperature, equilibrium pressure, molar fractions of xenon in the liquid and gaseous phases in equilibrium, and Henry's law coefficients, $H_{2,1}(T,p_1^{sat})$, are indicated.

Henry's law coefficients were calculated from experimental data as follows. Henry's law coefficients are usually defined as[17]

$$H_{2,1}(T,p) = \lim_{x_2 \to 0} \left[\frac{f_2(p, T, x_2)}{x_2} \right] \qquad (1)$$

Solubility of Xenon in *n*-Pentane and *n*-Hexane

J. Phys. Chem. B, Vol. 114, No. 48, 2010 **15899**

where f_2 is the fugacity of the solute (component 2) and x_2 its molar fraction in the liquid solution. The fugacity of component 2 can then be determined in the usual way[18]

$$f_2(p, T, x_2) = \varphi_2(p, T) y_2 p \qquad (2)$$

with

$$\varphi_2(p, T) = \exp\left[\frac{p(B_{22} + y_1^2 \delta_{12})}{RT}\right] \qquad (3)$$

where φ_2 is the fugacity coefficient of component 2, p is the vapor pressure of the saturated solution, and y_2 is the solute mole fraction in the vapor phase. B_{22} is the second virial coefficient of the solute, and δ_{12} is given by $2B_{12} - B_{11} - B_{22}$, where B_{11} is the second virial coefficient of the solvent and B_{12} is the solute–solvent crossed second virial coefficient.

The equilibrium compositions were calculated iteratively from experimentally measured quantities allowing for imperfection of the gaseous mixture. The process starts with initial guesses for the molar fractions in both phases and continues with the determination of the quantities of solute and solvent present in the two phases. The process converges rapidly, and coherent values for y_i and x_i are obtained after a few iterations. The calculation of Henry's law coefficients is then immediate using eqs 1–3. For comparison purposes, it is useful to express Henry's coefficients at the same pressure, namely, the vapor pressure of the pure solvent. The pressure dependence for $H_{2,1}$ can be expressed as[19]

$$H_{2,1}(T, p) = H_{2,1}(T, p_1^{\text{sat}}) \exp \int_{p_1^{\text{sat}}}^{p} \left[\frac{V_2^\infty(p, T)}{RT} dp\right] \qquad (4)$$

where V_2^∞ is the partial molar volume of the solute at infinite dilution and p_1^{sat} is the vapor pressure of the pure solvent.

The vapor pressure of *n*-pentane was taken from ref 20 and the molar volume calculated using the equation reported by Cibulka.[21] The second virial coefficients for pure *n*-pentane were taken from Dymond et al.[22] and for pure xenon from the compilation of Dymond and Smith.[23] The crossed virial coefficient for the mixture was estimated using the Tsonopoulos correlation.[24] As a first approximation, the partial molar volumes of xenon in *n*-pentane, necessary for calculation of the Henry's law coefficients (eq 4), were estimated using the method described by Tiepel and Gubbins.[25,26] This method has been applied to calculate the partial molar volume of several gases in water and proved to be accurate to within 3%. This uncertainty affects negligibly the values of the Henry's law constant.

Henry's law coefficients, $H_{2,1}(T, p_1^{\text{sat}})$, are plotted as a function of temperature in Figure 2. The solubility of xenon in *n*-pentane has been previously measured by Pollack and Himm[27] at 283.15 and 293.15 K and are also included in Figure 2. The values reported herein differ from these results, 1.7% and 0.5% respectively.

The dependence of the Henry's law coefficient in relatively narrow temperature ranges can be represented by the equation proposed by Clarke and Glew[28]
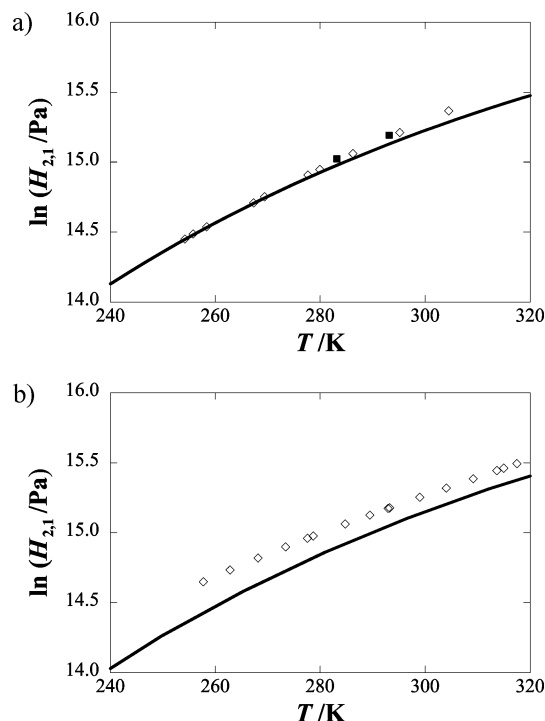
Figure 2. Henry's law coefficients for (a) xenon + *n*-pentane and (b) xenon + *n*-hexane. For xenon + *n*-pentane: ($\Diamond$) this work; (—) SAFT-VR results; (■) Pollack and Himm.[27] For xenon + *n*-hexane, the experimental results are from ref 13.

$$[\ln H_{2,1}(T, p_1^{\text{sat}})] = A_0 + \frac{A_1}{10^{-2}T/K} + A_2 \ln(10^{-2}T/K) + A_3(10^{-2}T/K) + A_4(10^{-2}T/K)^2 + \ldots \qquad (5)$$

The experimental results were fitted to eq 5, and the coefficients A_i are listed in Table 2. The relative deviations of the experimental results from the smoothing correlation do not exceed $\pm 0.25\%$, and the average absolute deviation (AAD) is 0.13%. The same procedure was applied to the solubility results of xenon in *n*-hexane from a previous work,[12] and the obtained coefficients are also included in Table 2.

The change in molar Gibbs energy when the solute is transferred, at temperature T, from the pure perfect gas state at standard pressure to the dilute state in the solvent (standard Gibbs energy of solvation)[29] is given by[18]

$$\Delta G_2^\circ(T, p_1^{\text{sat}}) = RT \ln\left(\frac{H_{2,1}(T, p_1^{\text{sat}})}{p^\circ}\right) \qquad (6)$$

where p° is the standard state pressure, considered as 101.325 kPa. The standard enthalpy and entropy of solvation can be obtained by calculating the corresponding partial derivatives of the Gibbs energy with respect to temperature at constant pressure. The result for the enthalpy of solvation at temperature T and at the vapor pressure of pure solvent is

$$\Delta H_2^\circ(T, p_1^{\text{sat}}) = -RT^2\left[\frac{d}{dT}\left(\frac{\ln H_{2,1}(T, p_1^{\text{sat}})}{p^\circ}\right) - \frac{V_2^\infty(T)}{RT}\left(\frac{dp_1^{\text{sat}}(T)}{dT}\right)\right] \qquad (7)$$

15900 *J. Phys. Chem. B, Vol. 114, No. 48, 2010*

Bonifácio et al.

TABLE 2: Coefficients for Eq 5 Correlating the Experimental Data for Xenon + *n*-Pentane and Xenon + *n*-Hexane Solutions

coefficients	xenon + *n*-pentane	xenon + *n*-hexane
A_0	+76.293	+74.287
A_1	−90.504	−86.314
A_2	−61.431	−54.874
A_3	+12.224	+10.012
AAD	+0.13%	0.5%

TABLE 3: Thermodynamic Functions of Solvation for Xenon in *n*-Pentane and *n*-Hexane[a]

T/K	$\Delta G_2°/\text{kJ mol}^{-1}$	$\Delta H_2°/\text{kJ mol}^{-1}$	$\Delta S_2°/\text{J K}^{-1}\text{ mol}^{-1}$
	xenon + *n*-pentane		
254.19	6.183	−11.084	−67.9
255.77	6.290	−11.096	−67.9
258.35	6.466	−11.125	−68.1
267.30	7.079	−11.332	−68.8
269.36	7.221	−11.402	−69.1
277.69	7.803	−11.774	−70.5
279.96	7.964	−11.900	−70.9
286.22	8.413	−12.300	−72.3
295.17	9.072	−13.009	−74.8
304.48	9.784	−13.916	−77.8
	xenon + *n*-hexane		
257.70	6.691	−9.470	−62.7
262.81	7.010	−9.352	−62.2
268.16	7.342	−9.275	−61.9
273.42	7.668	−9.246	−61.8
277.59	7.926	−9.255	−61.9
278.68	7.993	−9.262	−61.9
284.77	8.371	−9.338	−62.1
289.47	8.665	−9.439	−62.5
292.97	8.884	−9.538	−62.8
293.24	8.901	−9.546	−62.9
298.98	9.264	−9.754	−63.6
304.04	9.588	−9.983	−64.3
309.16	9.921	−10.25	−65.2
313.68	10.21	−10.53	−66.1
314.94	10.30	−10.61	−66.4
317.48	10.47	−10.79	−66.9
323.65	10.88	−11.26	−68.4
324.20	10.92	−11.31	−68.6
332.67	11.51	−12.06	−70.9

[a] $\Delta G_2°$ is the molar Gibbs energy of solvation, $\Delta H_2°$ the molar enthalpy of solvation, and $\Delta S_2°$ the molar entropy of solvation. The values are based on the ideal gas state at 101.325 kPa.

while the standard entropy of solvation is given by

$$\Delta S_2^o(T, p_1^{\text{sat}}) = -\frac{R \ln H_{2,1}(T, p_1^{\text{sat}})}{p^o} - RT\frac{d}{dT}\left(\frac{\ln H_{2,1}(T, p_1^{\text{sat}})}{p^o}\right) - V_2^\infty\left(\frac{dp_1^{\text{sat}}(T)}{dT}\right) \quad (8)$$

The thermodynamic functions of solvation were calculated from the Clarke and Glew smoothing equation for both xenon + *n*-pentane and xenon + *n*-hexane solutions. The results are listed in Table 3. No values obtained directly by calorimetric determinations could be found for comparison.

4. Theory

A quantitative interpretation of the results was performed using the statistical associating fluid theory for potentials of variable attractive range, SAFT-VR.[8] The SAFT-VR equation

TABLE 4: Optimized Square-Well Intermolecular Potential Parameters for *n*-Pentane, *n*-Hexane, and Xenon[a]

substance	m	λ	$\varepsilon/k_B/\text{K}$	σ/nm
xenon	1.00	1.478	243.3	0.3849
n-pentane	2.33	1.505	265.0	0.3931
n-hexane	2.67	1.432	283.1	0.4456

[a] m is the number of spherical segments in the model chain, λ the range, ε/k the depth of the potential well, and σ the diameter of each segment.

has been extensively tested against simulation data[30] for model fluids and successfully used to describe the phase equilibria of a wide range of industrially important experimental systems; for example, alkanes of low molecular weight through to simple polymers[31] and their binary mixtures,[32−34] perfluoroalkanes,[35] alcohols,[36] water,[37] and carbon dioxide,[38−41] have all been studied. The main expressions of the SAFT-VR equation of state for the square-well potential have been presented, and the reader is directed to the original reference for full details.[8] In the SAFT-VR approach, molecules are described as chains of m tangentially bonded hard spherical segments with the attractive interactions described by a potential of variable attractive range, such as the square-well potential used in this work. Each segment is characterized by three parameters, namely, the hard-sphere diameter σ and the depth ε and width λ of the potential well. For the *n*-alkanes, a simple empirical relationship between the number of carbon atoms n in the alkyl chain and the number of spherical segments m in the model chain has been proposed in earlier work:[42,43] $m = 0.33(C − 1) + 1$. Values of $m = 2.33$ and 2.67 are therefore used for *n*-pentane and *n*-hexane, respectively. A single sphere is naturally used to model the xenon atom. The remaining pure-substance parameters ε, σ, and λ are determined by fitting the theoretical expressions to the experimental vapor pressure and saturated liquid density data; the optimized parameters for xenon, *n*-pentane, and *n*-hexane[6,13] were determined in previous work and are presented in Table 4.

The study of phase equilibria in mixtures additionally requires determination of a number of unlike parameters. The unlike size parameter was calculated using the Lorentz combining rule

$$\sigma_{12} = (\sigma_{11} + \sigma_{22})/2 \quad (9)$$

and the unlike energy parameter from the Berthelot combining rule

$$\varepsilon_{ij} = \xi(\varepsilon_{ii}\varepsilon_{jj})^{1/2} \quad (10)$$

where deviations from the geometric mean can be allowed through the binary interaction parameter ξ. For both xenon + *n*-pentane and xenon + *n*-hexane systems we used $\xi = 1$, since with this approximation we were able to quantitatively describe a number of xenon + *n*-alkane systems.[5−7,13] The unlike range parameter was determined from the arithmetic mean

$$\lambda_{12} = \frac{\sigma_{11}\lambda_{11} + \sigma_{22}\lambda_{22}}{\sigma_{11} + \sigma_{22}} \quad (11)$$

In this way, the SAFT-VR approach becomes completely predictive in the sense that no parameters are fitted to experi-

Solubility of Xenon in *n*-Pentane and *n*-Hexane

J. Phys. Chem. B, Vol. 114, No. 48, 2010 **15901**

mental results for the mixtures being studied and are performed using solely pure-component parameters.

5. Computer Simulation

Henry's constants for xenon in *n*-pentane and *n*-hexane as a function of temperature were also obtained by computer simulation using Widom's test-particle insertion algorithm. The method uses Monte Carlo simulations to compute excess chemical potential ($\mu_2^{exc,\infty}$) of the solute 2 in the solvent 1 at infinite dilution, which in turn allows the calculation of Henry's constant by the well-known relation

$$H_{2,1}(T,p) = \lim_{x_2 \to 0} [RT\rho_1 \exp(^{\mu_2^{exc,\infty}}/_{RT})] \quad (12)$$

where $\mu_2^{exc\infty}$ is the excess chemical potential (the difference between the chemical potential of solute 2 in solvent 1 at infinite dilution and the chemical potential of pure species 2 at the ideal gas state), T is temperature, and ρ_1 is the density of pure solvent.

The excess chemical potential at infinite dilution is evaluated by

$$\mu_2^{exc,\infty} = -RT\frac{\langle V \exp(^{u_{TP}}/_{kT})\rangle_{NpT}}{\langle V \rangle_{NpT}} \quad (13)$$

where u_{TP} is the interaction energy of the test particle with a configuration of solvent molecules, V is the volume of solvent in a given configuration, and {NpT denotes an isothermal−isobaric ensemble average.

The computer simulations were performed using the MCCCS Towhee Monte Carlo molecular simulation package, version 6.2.2.[44] The force field used to describe both *n*-alkanes was based on TraPPE-UA,[45] whose main characteristics are fixed bond lengths, harmonic style angle bending terms, quadratic torsion terms for the intramolecular interactions, and the intermolecular terms are modeled by Lennard−Jones potentials centered on the carbon atoms. This is a united atom force field, which means that CH_n groups are modeled as single pseudoatoms; however, the nonbonded parameters used were not those proposed by Martin et al.[41] Although TraPPE-UA produces good results for the excess thermodynamic functions of mixtures involving light *n*-alkanes (ethane, propane, and *n*-butane) and xenon,[46] vapor pressures of these *n*-alkanes as pure compounds were not well predicted, particularly at low temperatures. Recently, Laginhas et al.[47] carried out an optimization of the nonbonded parameters of CH_3 and CH_2 within the TraPPE-UA framework in order to obtain agreement between experimental and simulation results of vapor pressures and densities for the lightest *n*-alkanes (except methane) at low temperatures. More specifically, the procedure used by Laginhas was as follows: a trial and error optimization of nonbonded CH_3 parameters was done in order to match experimental and simulation results of vapor pressure and density for ethane. Using this pair of parameters, the CH_2 ones were determined by matching the same results for propane. Then, ε and σ for CH_3 and CH_2, optimized in this way, were used to predict vapor pressures and densities for *n*-butane at low temperatures, giving a reasonable agreement between simulation and experimental results. Furthermore, using the optimized pairs of potential parameters, the authors were able to predict liquid−vapor equilibrium diagrams for xenon + ethane, xenon + propane, and xenon + *n*-butane binary mixtures. Xenon parameters have also been optimized by the

TABLE 5: Nonbonded Parameters for Each Interaction Site Used in This Work for Computer Simulation Calculations Compared with the Original Ones

	this work		original	
	$(\varepsilon/k_B)/K$	$\sigma/\text{Å}$	$(\varepsilon/k_B)/K$	$\sigma/\text{Å}$
CH_3[31]	100.75	3.787	98	3.75
CH_2[31]	47.2	4.03	46	3.95
Xe[34]	226.3	3.948	227.9	3.948

same trial and error procedure, using the Lennard−Jones-type potential from Bohn et al.[48] as the starting point. However, in the case of the three *n*-alkanes studied, no unique pair of parameters for each interaction site was obtained for the entire temperature range tested. Two sets of parameters have been proposed: one for the low-temperature (up to 210 K) limit and the other for the high-temperature limit. In this work we use the high-temperature set of parameters for the *n*-alkanes and the unique set for xenon both obtained by Laginhas et al. The parameters used in this work are shown in Table 5, where they are also compared with the original ones. The unlike parameters were obtained using the Lorentz−Berthelot combination rule, which means that no experimental results were needed to predict Henry's constants.

The calculations were carried out in the *NpT* ensemble with a single box having side lengths of approximately 35−40 Å and containing 300 solvent molecules. A 12 Å cutoff radius was used in the interaction calculations, and the neglect of long-range interactions beyond the cutoff radius was compensated by application of analytic tail corrections. Coulombic interactions were not considered, since all the molecules studied are neutral and apolar. In each simulation, a preliminary solvent equilibration run of 50 000 MC cycles (each cycle consisting of a number of moves equal to the number of molecules in the system) was done, followed by a production run consisting of another 200 000 MC cycle, which were divided into 20 blocks in order to calculate standard deviations. One thousand insertions of solute test particle were done for each MC production cycle (a total of 2×10^8 insertions per run). The Monte Carlo moves consisted of simulation box volume changes, coupled−decoupled configurational−bias regrowths, translations of the center of mass, rotations about the center of mass, and configurational−bias molecule reinsertions in the simulation box. Henry's constant calculations were done as a function of temperature from 250 to 305 K for xenon + *n*-pentane and 335 K for xenon + *n*-hexane at 5 K intervals. The system pressure was fixed to a value of 100 kPa. Henry's constants obtained by computer simulation were corrected to the solvent vapor pressure so that they can be compared with experimental results. The correction was done by the same procedure used to correct the experimental Henry's constants.

6. Discussion

The results of the SAFT-VR calculations for the xenon + *n*-pentane and xenon + *n*-hexane systems are presented in Figure 2 and compared with the experimental results. The Henry's constants were calculated from the chemical potential of xenon in the solvent at infinite dilution.[49] As can be seen from the figure, the SAFT-VR predictions are in excellent agreement with the experimental results for the xenon + *n*-pentane mixture. In the case of xenon + *n*-hexane the theoretical results underestimate the experimental Henry's coefficients by ∼10%. It should be kept in mind, however, that no deviations from the Lorentz−Berthelot combining rules were introduced, and there-

TABLE 6: Monte Carlo Results of Henry's Constants for the Dissolution of Xenon in *n*-Pentane As a Function of Temperature, Henry's Constants at Saturation Pressure of the Solvent, and Henry's Constant Standard Deviations
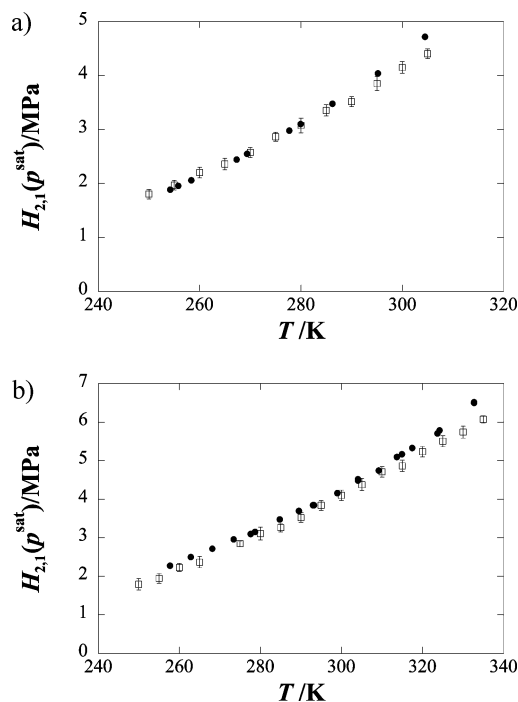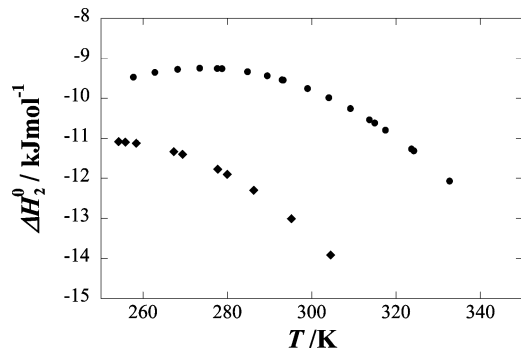
T/K	$H_{2,1}/MPa$	p^{sat}/kPa	$H_{2,1}^{psat}/MPa$	$\delta H_{2,1}^{psat}/MPa$
250	1.81	7.538	1.80	0.087
255	1.97	9.919	1.97	0.085
260	2.21	12.89	2.20	0.098
265	2.36	16.56	2.36	0.10
270	2.58	21.05	2.57	0.096
275	2.87	26.48	2.86	0.084
280	3.08	32.99	3.07	0.14
285	3.36	40.73	3.35	0.10
290	3.52	49.87	3.52	0.091
295	3.85	60.57	3.85	0.13
300	4.15	73.01	4.15	0.11
305	4.40	87.39	4.40	0.091

TABLE 7: Monte Carlo Results of Henry's Constants for the Dissolution of Xenon in *n*-Hexane As a Function of Temperature, Henry's Constants at Saturation Pressure of the Solvent, and Henry's Constant Standard Deviations

T/K	$H_{2,1}/MPa$	p^{sat}/kPa	$H_{2,1}^{psat}/MPa$	$\delta H_{2,1}^{psat}/MPa$
250	1.80	1.504	1.79	0.15
255	1.95	2.078	1.95	0.13
260	2.23	2.829	2.23	0.11
265	2.37	3.799	2.37	0.14
270	2.67	5.035	2.66	0.12
275	2.85	6.591	2.85	0.077
280	3.11	8.530	3.11	0.17
285	3.27	10.922	3.26	0.11
290	3.53	13.843	3.52	0.12
295	3.84	17.378	3.84	0.13
300	4.11	21.620	4.10	0.14
305	4.38	26.671	4.38	0.16
310	4.72	32.637	4.71	0.14
315	4.87	39.637	4.86	0.15
320	5.24	47.794	5.23	0.13
325	5.51	57.239	5.50	0.14
330	5.74	68.112	5.74	0.16
335	6.07	80.558	6.07	0.090

Figure 3. Henry's constants for (a) xenon + *n*-pentane and (b) xenon + *n*-hexane obtained by computer simulation (□, with their corresponding error bars) in comparison with experimental results (●).

Figure 4. Standard molar enthalpies of solvation $\Delta H_2°$ for (◆) xenon + *n*-pentane and (●) xenon + *n*-hexane as a function of temperature.

fore, agreement with experimental data could be improved by adjusting the cross-interaction energy; however, this would detract from the comparisons being made to the *n*-alkanes.

A theoretical interpretation of the results was also attempted by Monte Carlo simulation. Henry's constants as a function of temperature obtained by simulation are presented in Table 6 for xenon + *n*-pentane and Table 7 for xenon + *n*-hexane, both with their standard deviations. The comparison with experimental results is shown, respectively, in Figure 3a and 3b. In the case of xenon + *n*-pentane, the agreement between simulation and experimental results is remarkable, in particular at the lowest temperatures. In the high-temperature limit, the deviations between simulation and experimental results seem to increase, in any case not exceeding 7%. For xenon in hexane, the agreement is quite good, also showing more pronounced deviations at the highest temperatures; the maximum deviation from experimental results is 9%. The most interesting feature of the results is the fact that the prediction was done with a rather simple model for the *n*-alkanes. The xenon + *n*-hexane system is much better described by this model than by the OPLS all-atom force field, as used by Bonifácio et al.[13] As shown in this work, modeling *n*-alkanes with force fields based on implicit hydrogen atoms can be quite successful for vapor−liquid equilibrium predictions. It is also interesting to note the resemblance between the two models underlying the two theoretical treatments (TraPPE-UA and SAFT-VR). In both

cases, the *n*-alkane molecules are taken as a chain of spherical segments interacting through a spherical symmetric potential, though the intramolecular interactions within the *n*-alkane chain are not considered explicitly in the SAFT model. The xenon particle is also modeled as a sphere of practically the same diameter. As can be seen, the results of both treatments are very similar and both are able to capture the similarity of thermodynamic behavior between xenon and the *n*-alkanes.

The standard enthalpy of solvation for xenon + *n*-pentane and xenon + *n*-hexane solutions is plotted in Figure 4 as a function of temperature. As can be seen, the enthalpy of solvation slightly increases at lower temperatures, goes through a maximum, and then decreases at higher temperatures. The temperature at which the solvation enthalpy is maximum is 254.5 K for xenon + *n*-pentane) and 275 K for xenon + *n*-hexane. Interestingly, these temperatures correspond to 0.54 reduced temperature for both solvents and is very close to the reduced temperature at which H^E ($x = 0.5$) becomes zero for mixtures of *n*-alkanes (Figure 1).

The dissolution process of a solute in a solvent is often described as the combination of two contributions: (1) formation of a cavity with the appropriate size and shape to host the solute

Solubility of Xenon in *n*-Pentane and *n*-Hexane

J. Phys. Chem. B, Vol. 114, No. 48, 2010 **15903**
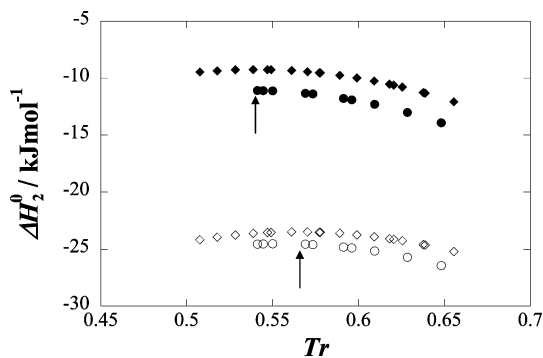
Figure 5. Standard molar enthalpies of solvation, ΔH_2° (filled symbols), and enthalpies of interaction, H_{int} (open symbols), for xenon + *n*-pentane (circles) and xenon + *n*-hexane (diamonds) as a function of reduced temperature. The arrows locate maxima.

7. Conclusion

Solubilities of xenon in *n*-pentane, expressed as Henry's law coefficients, were measured between 254 and 304 K with an estimated accuracy of 0.15%. The thermodynamic functions of solvation such as the standard Gibbs energy, enthalpy, and entropy of solvation have been calculated from Henry's law coefficients and its temperature dependence for xenon + *n*-pentane solutions and for xenon + *n*-hexane from a previous work. The molar enthalpy of solvation was decomposed into its cavity and interaction contributions. For both systems the enthalpy of interaction shows a maximum at a reduced temperature of 0.57, the same reduced temperature at which the excess enthalpy for equimolar mixtures of *n*-alkanes change from positive to negative. This result provides a further example of the similarity between the xenon + *n*-alkane interaction and the *n*-alkane + *n*-alkane interactions.

The solubility results were modeled using the SAFT-VR equation and molecular simulation. The theoretical results predict closely the experimental solubility of xenon in *n*-pentane and *n*-hexane over the range of temperatures studied using simple Lorentz−Berthelot combining rules for the unlike interactions.

molecule and (2) interaction between the solute molecules and the solvent molecules within its coordination sphere. Energetically, cavity formation is often identified with the vaporization enthalpy of the solvent, ΔH_{vap}, corrected for the change in size and shape of the cavity. Irrespectively of the model used to calculate the enthalpy of cavity formation, H_{cav}, the solute−solvent enthalpy of interaction, H_{int}, can then be obtained from the solvation enthalpy as

$$H_{int} = \Delta H_2^0 - H_{cav} \tag{12a}$$

In this work we calculated the enthalpy of cavity formation for xenon in *n*-pentane and *n*-hexane following the procedure proposed by Sinonaglu[50]

$$H_{cav} = \frac{S_s}{S_S} \Delta_{vap} H \tag{13a}$$

where S_s/S_S represents the ratio of the surfaces of the solute and solvent cavities and can be calculated from partial molar volumes at infinite dilution of the solute in the solvent, molar volumes of the solvent, and simple geometrical considerations.

The calculated interaction enthalpies, H_{int}, are plotted in Figure 5 as a function of the reduced temperature. As can be seen, the interaction enthalpy of xenon and *n*-pentane is stronger (more negative) than that with *n*-hexane. This reflects the higher percentage of CH3 groups in the *n*-pentane molecule, with which xenon interacts more strongly than with CH2 groups.[51] However, perhaps more interestingly, it is also seen that the interaction enthalpy of xenon with both alkanes shows a maximum at a reduced temperature of 0.57. As previously explained, mixtures of *n*-alkanes mix with positive excess enthalpies at low temperature that decrease with increasing temperature, go through zero, and become negative at higher temperatures. The temperature at which H^E ($x = 0.5$) becomes negative is found to be within 0.57 and 0.59 for all systems (Figure 1b).

It should be emphasized that separating the experimental solvation enthalpy into contributions from cavity formation within the solvent and solute−solvent interaction provides a clear indication that the explanation for the observed behavior should be at the level of the cross interaction. While the reason for this behavior is not clear, the present result is a further example of the similarity between the xenon + *n*-alkane interaction and the *n*-alkane + *n*-alkane interactions.

References and Notes

(1) Lynch, C., III; Baum, J.; Tenbrinck, R. *Anesthesiology* **2000**, *92*, 865–868.

(2) Pollack, G. L. *J. Chem. Phys.* **1981**, *75*, 5875–5878.

(3) Pollack, G. L. *Science* **1991**, *251*, 1323–1330.

(4) Lim, Y.-H.; King, A. D., Jr. *J. Phys. Chem.* **1993**, *97*, 12173–12177.

(5) Dias, L. M. B.; McCabe, C.; Filipe, E. J. M.; Calado, J. C. G. *J. Phys. Chem. B* **2004**, *108*, 7377–7381.

(6) Filipe, E. J. M.; Gomes de Azevedo, E. J. S.; Martins, L. F. G.; Soares, V. A. M.; Calado, J. C. G.; McCabe, C.; Jackson, G. *J. Phys. Chem. B* **2000**, *104*, 1315–1321.

(7) Filipe, E. J. M.; Martins, L. F. G.; Calado, J. C. G.; McCabe, C.; Jackson, G. *J. Phys. Chem. B* **2000**, *104*, 1322–1325.

(8) Gil-Villegas, A.; Galindo, A.; Whitehead, P. J.; Mills, S. J.; Jackson, G.; Burgess, A. N. *J. Chem. Phys.* **1997**, *106*, 4168–4186.

(9) Personal communication.

(10) Martins, L. F. G. Ph.D. Thesis, Instituto Superior Técnico, Lisboa, Portugal, 1999.

(11) Dos Ramos, M. C.; Blas, F. J. *J. Phys. Chem. B* **2005**, *109*, 12145–12153.

(12) Hildebrand, J. H.; Prausnitz, J. M.; Scott, R. L. *Regular and Related Solutions*; Van Nostrand Reinhold: New York, 1970; pp 111−141.

(13) Bonifácio, R. P.; Costa Gomes, M. F.; Filipe, E. J. M. *Fluid Phase Equilib.* **2002**, *193*, 41–51.

(14) Bonifácio, R. P.; Filipe, E. J. M.; McCabe, C.; Costa Gomes, M. F.; Pádua, A. A. H. *Mol. Phys.* **2002**, *101*, 2547–2553.

(15) Ambrose, D.; Walton, J. *Pure Appl. Chem.* **1989**, *61*, 1395–1403.

(16) Carnicer, J.; Gibanel, F.; Urieta, J. S.; Gutierrez Losa, C. *Rev. Acad. Cienc. Zaragoza* **1979**, *34*, 115–122.

(17) Smith, J. M.; Van Ness, H. C.; Abbott, M. M. *Introduction to Chemical Engineering Thermodynamics*, 5th ed.; McGraw-Hill: New York, 1996.

(18) Rettich, T. R.; Handa, Y. P.; Battino, R.; Wilhelm, E. *J. Phys. Chem.* **1981**, *85*, 3230–3237.

(19) Benson, B. B.; Krause, D. J., Jr. *J. Sol. Chem.* **1989**, *18*, 803–821.

(20) Lemmon, E. W.; Goodwin, A. R. H. *J. Phys. Chem. Ref. Data* **2000**, *29*, 1.

(21) Cibulka, I. *Fluid Phase Equilib.* **1993**, *89*, 1–18.

(22) Dymond, J. H.; Cholinski, J. A.; Szafranskiand, A.; Wyrzykowska-Stankiewicz, D. *Fluid Phase Equilib.* **1986**, *27*, 1–13.

(23) Dymond, J. H.; Smith, E. B. *The Virial Coefficients of Pure Gases and Mixtures*; Clarendon Press, Oxford, 1980.

(24) Poling, B. E.; Prausnitz, J. M.; O'Connell, J. P. *The Properties of Gases and Liquid*, 5th ed.; McGraw-Hill: New York, 2001.

(25) Tiepel, E. W.; Gubbins, K. E. *Can. J. Chem. Eng.* **1972**, *50*, 361–364.

(26) Tiepel, E. W.; Gubbins, K. E. *J. Phys. Chem.* **1972**, *76*, 3044–3049.

(27) Pollack, G. L.; Himm, J. F. *J. Chem. Phys.* **1982**, *77*, 3221–3229.

(28) Clarke, E. C. W.; Glew, D. N. *Trans. Faraday Soc.* **1966**, *62*, 539–545.

(29) Costa Gomes, M. F.; Grolier, J. P. *Phys. Chem. Chem. Phys.* **2001**, *3*, 1047–1052.

(30) Galindo, A.; Davies, L. A.; Gil-Villegas, A.; Jackson, G.; Calero, S.; Lago, S. *Phys. Rev. E* **1998**, *57*, 2035. McCabe, C.; Gil-Villegas, A.; Jackson, G. *Chem. Phys. Lett.* **1999**, 303–27. Davies, L. A.; Gil-Villegas, A.; Jackson, G. *J. Chem. Phys.* **1999**, 111–8659. Kalyuzhnyi, Y.; McCabe, C.; Whitebay, E.; Cummings, P. T. *J. Chem. Phys.* **2004**, 121–8128.

(31) McCabe, C.; Jackson, G. *Phys. Chem. Chem. Phys.* **1999**, *1*, 2057. McCabe, C.; Galindo, A.; Garcia-Lisbona, M. N.; Jackson, G. *Ind. Eng. Chem. Res.* **2001**, *40*, 3835. McCabe, C.; Kiselev, S. B. *Ind. Eng. Chem. Res.* **2004**, *43*, 2839.

(32) McCabe, C.; Galindo, A.; Gil-Villegas, A.; Jackson, G. *Int. J. Thermophys.* **199819**, 1511. McCabe, C.; Gil-Villegas, A.; Jackson, G. *J. Phys. Chem. B* **1998**, *102*, 4183. Galindo, A.; Florusse, L. J.; Peters, C. J. *Fluid Phase Equilib.* **1999**, *160*, 123. Sun, L. X.; Zhao, H. G.; Kiselev, S. B.; McCabe, C. *J. Phys. Chem. B* **2005**, *109*, 9047. Zhao, H. G.; Morgado, P.; McCabe, C.; Gil Villegas, A. *J. Phys. Chem. B* **2006**, *110*, 24083.

(33) Sun, L. X.; Zhao, H. G.; Kiselev, S. B.; McCabe, C. *Fluid Phase Equilib.* **2005**, *228*, 275.

(34) Dias, L. M. B.; Bonifacio, R. P.; Filipe, E. J. M.; Calado, J. C. G.; McCabe, C.; Jackson, G. *Fluid Phase Equilib.* **2003**, *205*, 163. Pollock, M.; Adjiman, C. S.; Galindo, A.; Jackson, G.; Filipe, E. J. M. *Ind. Eng. Chem. Res.* **2009**, *48*, 2188.

(35) McCabe, C.; Galindo, A.; Gil-Villegas, A.; Jackson, G. J. *Phys. Chem. B* **1998**, *102*, 8060. Bonifacio, R. P.; Filipe, E. J. M.; McCabe, C.; Gomes, M. F. C.; Padua, A. A. H. *Mol. Phys.* **2002**, *100*, 2547. Morgado, P.; McCabe, C.; Filipe, E. J. M. *Fluid Phase Equilib.* **2005**, *228*, 389. Morgado, P.; Zhao, H. G.; Blas, F. J.; McCabe, C.; Rebelo, L. P. N.; Filipe, E. J. M. *J. Phys. Chem. B* **2007**, *111*, 2856.

(36) Watson, G.; Latitte, T.; Zeberg-Mikkelsen, C. K.; Baylaucq, A.; Bessieres, D.; Boned, C. *Fluid Phase Equilib.* **2007**, *253*, 80. Castro-Marcano, F.; Olivera-Fuentes, C. G.; Colina, C. M. *Ind. Eng. Chem. Res.*

2008, *47*, 8894. Clark, G. N. I.; Galindo, A.; Jackson, G.; Rogers, S.; Burgess, A. N. *Macromolecules* **2008**, *41*, 6582.

(37) McCabe, C.; Galindo, A.; Cummings, P. T. J *Phys. Chem. B* **2003**, *107*, 12307. Valtz, A.; Chapoy, A.; Coquelet, C.; Paricaud, P.; Richon, D. *Fluid Phase Equilib.* **2004**, *226*, 333. Clark, G. N. I.; Haslam, A. J.; Galindo, A.; Jackson, G. *Mol. Phys.* **2006**, *104*, 3561. Zhao, H. G.; McCabe, C. *J. Chem. Phys.* **2006**, *125*, 4504.

(38) Blas, F. J.; Galindo, A. *Fluid Phase Equilib.* **2002**, *194−197*, 501. Sun, L. X.; Zhao, H. G.; Kiselev, S. B.; McCabe, C. *Fluid Phase Equilib.* **2005**, *228*, 275.

(39) Galindo, A.; Blas, F. J. *J. Phys. Chem. B* **2002**, *106*, 4503.

(40) dos Ramos, M. C.; Blas, F. J.; Galindo, A. *J. Phys. Chem. C* **2007**, *111*, 15924.

(41) dos Ramos, M. C.; Blas, F. J.; Galindo, A. *Fluid Phase Equilib.* **2007**, *261*, 359.

(42) Jackson, G.; Gubbins, K. E. *Pure Appl. Chem.* **1989**, *61*, 1021.

(43) Archer, A. L.; Amos, M. D.; Jackson, G.; McLure, I. A. *Int. J. Thermophys.* **1996**, *17*, 201.

(44) http://towhee.sourceforge.net.

(45) Martin, M. G.; Siepmann, J. I. *J. Phys. Chem. B* **1998**, *102*, 2569.

(46) Palace Carvalho, A. J.; Prates Ramalho, J. P.; Martins, L. F. G. *J. Phys. Chem. B.* **2007**, *102*, 2569.

(47) Laginhas, C. E. C.; Palace Carvalho, A. J.; Prates Ramalho, J. P.; Martins, L. F. G. *Proceedings of the 10th International Chemical and Biological Engineering Conference, CHEMPOR*, Braga, Portugal, Sept 4−6, 2008.

(48) Bohn, M.; Lago, S.; Fischer, J.; Kohler, F. *Fluid Phase Equilib.* **1985**, *23*, 137.

(49) Ghonasgi, D.; Llanorestrepo, M.; Chapman, W. G. *J. Chem. Phys.* **1993**, *98*, 5662.

(50) Sinanoglu, O. *Mol. Interact.* **1982**, *3*, 283.

(51) Bonifácio, R. Ph.D. Thesis, Instituto Superior Técnico, 2004.